Journal of Solid State Chemistry **159,** 268–280 (2001)
doi:10.1006/jssc.2001.9156, available online at http://www.idealibrary.com on IDEAL®

Magnetic Exchange between Orbitally Degenerate Metal Ions: The Problem of Magnetic Anisotropy

J. J. Borrás-Almenar and E. Coronado[1]

Departamento de Química Inorgánica, Instituto de Ciencia Molecular, Universidad de Valencia, C/Dr. Moliner 50, 46100-Burjassot (Valencia), Spain
E-mail: juan.j.borras@uv.es; eugenio.coronado@uv.es

J. M. Clemente-Juan

Laboratoire de Chimie de Coordination 205, Route de Narbonne, 31077 Toulouse Cedex 04, France
E-mail: clemente@lcc-toulouse.fr

and

A. V. Palii and B. S. Tsukerblat

Quantum Chemistry Department Institute of Chemistry, Academy of Sciences of Moldova, MD-2028 Kishinev, Moldova
E-mail: root@uuquatn.asm.md; clara_jignea@mdl.net

Received March 21, 2001

IN DEDICATION TO THE LATE PROFESSOR OLIVIER KAHN FOR HIS POINEERING CONTRIBUTIONS TO THE FIELD OF MOLECULAR MAGNETISM

In this paper we show that a strong magnetic anisotropy appears in exchange mixed–valence clusters containing orbitally degenerate metal ions. Combining an effective Hamiltonian approach with the technique of the irreducible tensor operators (ITO) and pseudoangular momentum representation we have solved the problem of magnetic exchange in localized and delocalized (mixed–valence) systems with different overall symmetries (D_{2h}, D_{3h}, D_{4h}). The energy pattern as well as the character of the magnetic anisotropy is closely related to the ground term of the ions, electron transfer pathways, and overall symmetry of the system being affected also by the local crystal fields, spin–orbital interactions, and vibronic interactions. Special attention is paid to the origin of the magnetic anisotropy in the face–shared (D_{3h}) binuclear unit $[Ti_2Cl_9]^{-3}$. For this case a very good agreement between calculated and measured $\chi(T)$ is obtained. © 2001 Academic Press

Key Words: **magnetic exchange; mixed-valency; orbital degeneracy; magnetic anisotropy; vibronic interaction.**

1. INTRODUCTION

Molecular assemblies containing a finite number of exchange coupled magnetic ions (molecular clusters) are currently important for several areas of research such as solid state chemistry and molecular chemistry, magnetism, and biochemistry. In particular we are interested in the possibility of using simple molecular clusters as magnets of nanometer size possessing the unusual magnetic properties of superparamagnetic–like behavior and quantum tunneling of magnetization (1–6). Organic molecules containing unpaired electrons are also being used for obtaining building blocks for molecular-based magnets (7–11). Magnetic clusters of transition metal ions are relevant in biochemistry (e.g., ferredoxins (12), photosystem II (13), and the storage protein ferritin (14, 15).

The interplay between the electron delocalization and magnetic interactions plays a crucial role in the properties of many mixed–valence (MV) compounds of current interest in solid state chemistry and physics (bulk magnets, superconductors) as well as in inorganic chemistry (heteropolyblues) (16–20). Recently molecular materials exhibiting the coexistence of these two electronic processes, for example, the discovery of the first molecular material with coexistence of ferromagnetism and metallic conductivity have been reported (21).

In 1951, Zener (22) proposed a new exchange mechanism, namely double exchange, that ferromagnetically couples two spins through the hopping of an *extra electron.* This mechanism was used by Zener to explain the ferromagnetism observed in the manganites MV oxides, a family of compounds that is currently creating much excitement in

[1] To whom correspondence should be addressed.

0022-4596/01 $35.00

solid sate chemistry due to the observation of giant magnetoresistance. Anderson and Hasegawa (23) solved the double-exchange problem for a dimer by deducing the spin–dependence for the double-exchange splitting. More recently, the concept of double exchange was applied to more complex systems (trimers and tetramers; see review papers (12, 24, 25)). Finally, a general solution of the problem of the double exchange was found for the high–nuclearity MV clusters in which an arbitrary number of electrons are delocalized over a network of magnetic metal sites (26).

A vast number of polynuclear compounds (exchange clusters), low-dimensional systems, and extended magnetic materials have been studied in the framework of the isotropic exchange (Heisenberg–Dirac–van Vleck, HDDV) model (26–33). This model is valid if the constituent ions are orbitally nondegenerate (spin systems). For the spin systems the anisotropic contributions (local anisotropy, antisymmetric exchange, etc.) are relatively small and usually can be considered in a perturbational way (24). The theory of the double exchange, proposed by Anderson and Hasegawa, and the subsequent studies are essentially based on the assumption that the metal ions (in both oxidation degrees) are orbitally nondegenerate. This assumption leads to the conclusion that double exchange is magnetically isotropic.

The situation is quite different when the orbital angular momenta of the constituents ions are not quenched by the low–symmetry crystal fields such that the orbital degeneracy remains in a high–symmetric ligand surroundings. A model example is provided by the dimers $[Ti_2Cl_9]^{-3}$ and $[Ti_2Br_9]^{-3}$ in which two trivalent titanium ions are interacting through halide bridging atoms (34). Almost two decades ago, Kahn and co-workers discovered that one of the most spectacular features of the magnetic behavior of the $[Ti_2Cl_9]^{-3}$ entity is the significant magnetic anisotropy (35, 36). In their paper (35) they introduced a simple form of the orbital interaction.

For the first time Khomskii and Kugel derived a kinetic exchange Hamiltonian for orbitally degenerate ions and created a new field in solid state physics, namely orbital ordering in solids (see the review paper of Khomskii and Kugel (37) and references therein). Motivated by the work of Kahn, Drillon and Georges (38) and, independently, Leuenberger and Güdel (39) developed the theory of kinetic exchange in dimers formed by orbitally degenerate ions (d^1–d^1 and d^2–d^2 configurations). Unfortunately, these simplified models proved to be of limited applicability for real systems.

In a recent paper (40) we proposed a more general approach to the problem of the kinetic exchange between orbitally degenerate multielectron transition metal ions. Our consideration takes explicitly into account the complex energy spectrum of charge transfer crystal field states deduced by the Tanabe–Sugano diagrams. Taking advantage of these symmetry arguments, we have deduced the effective exchange Hamiltonian in its general form for an arbitrary overall symmetry of the dimer that takes into account all relevant electron transfer pathways. All parameters of the Hamiltonian incorporate physical characteristics of the magnetic ions in their crystal surroundings.

The application of the developed approach enabled us to explain the magnetic anisotropy of the $[Ti_2Cl_9]^{-3}$ binuclear unit (41). In another paper (42) we have proposed a theory of the double exchange in MV dimers in which one or both transition metal ions possess orbitally degenerate ground states. Both kinds of systems exhibit magnetic anisotropy arising from the orbital interactions. As distinguished from the spin systems, the magnetic anisotropy of the orbital nature proves to be strong and manifests itself in the new magnetic properties of the systems with orbital degeneracy.

In this paper we focus on exchange and mixed–valence containing orbitally degenerate ions with the main emphasis on the magnetic anisotropy. Let us begin with the relative simple spin clusters. Figure 1 shows a sketch of the orbital states for an MV (delocalized) d^n–d^{n+1} dimer (Fig. 1a) and for an exchange (localized) d^n–d^n cluster (Fig. 1b). In the former case, an *extra* electron moves freely between two non degenerate orbitals a and b and the effective transfer parameter is spin–dependent due to double exchange (23):

$$t(S) = t_o(S + \tfrac{1}{2}), \qquad [1]$$

where $t_o = t(2S_o + \frac{1}{2})$. S_o is the spin of the core and $t = \langle a|\hat{h}|b\rangle$ is the one–electron transfer integral ($\hat{h}$ is the one–particle part of the Hamiltonian). The kinetic exchange also arises from the electron delocalization. Figure 1b illustrates the contribution arising from the jump from the half-filled orbital b_n to the empty orbital a. As distinguished from the MV system, this jump is constrained by the intersite Coulomb repulsion U so that the exchange in the localized system appears as a second-order effect:

$$\frac{t^2(S)}{U} = \frac{t_o^2}{U} S(S+1) + \frac{t_o^2}{4U}. \qquad [2]$$

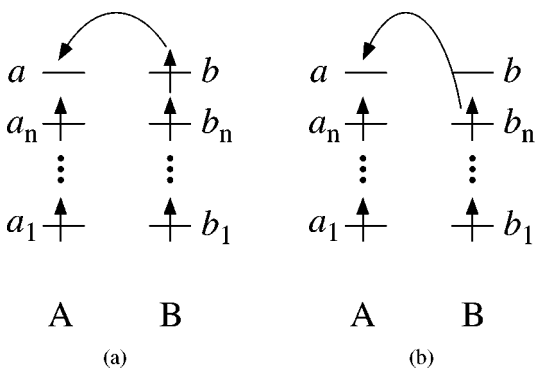

FIG. 1. Orbital schemes for mixed-valence (a) and exchange (b) clusters.

This spin dependence gives rise to the HDDV model:

$$\mathbf{H}_{\text{ex}} = -2J\mathbf{S}_A\mathbf{S}_B. \qquad [3]$$

For the subsequent considerations, it is important to note that in MV systems containing magnetically isotropic spin ions, the energy levels only depend upon full spin S, and are independent of the magnetic quantum numbers M_L. The HDVV exchange as a second-order correction also proves to be isotropic, and the effective spin Hamiltonian (Eq. [3]) contains the scalar product of spin operators.

In contrast, the orbitally degenerate ions carry orbital angular momenta that are coupled with each other and also with the spin subsystem. In fact, as distinguished from the spin, the orbital states in the case of degeneracy are subjected to the action of the crystal field so that the orbital angular momenta cannot be freely aligned along the external magnetic field. This effect leads to a strong magnetic anisotropy. By using relatively simple examples, we will illustrate the main physical conditions determining the character of magnetic anisotropy arising from the orbital interactions.

2. MIXED-VALENCE DIMERS

2.1. Double Exchange in Pseudo–angular Momentum Representation

Let us consider MV dimers of different topology containing octahedrally coordinated metalions in orbitally triplet states T_1 or T_2 (terms $^{2S+1}T_1$ and $^{2S+1}T_2$) (42). The T–P isomorphism allows us to assign $T_{1(2)}$ basis to the $|lm\rangle$ states with $l = 1$,

$$\xi(\alpha) = -\frac{1}{\sqrt{2}}(|11\rangle - |1-1\rangle)$$

$$\eta(\beta) = -\frac{i}{\sqrt{2}}(|11\rangle + |1-1\rangle)$$

$$\zeta(\gamma) = |10\rangle, \qquad [4]$$

where $\alpha \propto L_x$, $\beta \propto L_y$, $\gamma \propto L_z$ are the standard notations for T_1 basis; $\xi \propto yz$, $\eta \propto xz$, $\zeta \propto xy$ represents T_2 basis.

This transformation is of the same form as those relating p_x, p_y, and p_z functions with $|lm\rangle$ basis and possessing genuine orbital angular momentum $l = 1$.

Now we can use the following labeling for the ground terms: $\tilde{S}\tilde{L}$ for d^{n+1} ions and $\bar{S}\bar{L}$ for d^n ions, with $\bar{L} = 1(\tilde{L} = 1)$ for orbital triplets and $\bar{L} = 0$ $(\tilde{L} = 0)$ for orbital singlets.

Pseudo–angular momentum representation provides the opportunity to apply the efficient angular momentum technique for treating the double-exchange problem and also provides a clear insight into the magnetic anisotropy of such a system. We define the angular momenta coupled basis for each localization of the extra electron, namely, $|\tilde{S}_A\tilde{L}_A, \bar{S}_B\bar{L}_B, SM_SLM_L\rangle, |\bar{S}_A\bar{L}_A, \tilde{S}_B\tilde{L}_B, SM_SLM_L\rangle$, where S and L are the total spin and total orbital angular momentum of the dimer. This basis corresponds to the Russell-Saunders scheme for pseudo–angular momenta and spins in a dimer. It can be built with the use of the Clebsh–Gordan coefficients.

The calculation of the matrix element of the double exchange for the high–spin systems with less than half filled shell gives the result:

$$(\tilde{S}_A\tilde{L}_A, \bar{S}_B\bar{L}_B, SLM_SM_L\,|\mathbf{V}_{AB}|\,\bar{S}_A\bar{L}_A, \tilde{S}_B\tilde{L}_B, S'L'M'_SM'_L\rangle$$

$$= \delta_{SS'}\delta_{M_SM'_S}\frac{(-1)^f[\langle\tilde{S}\tilde{L}\|T_{1\frac{1}{2}}\|\bar{S}\bar{L}\rangle]^2}{2(S_o+1)(2S_o+1)}(S+\tfrac{1}{2})$$

$$\times\sqrt{2L'+1}\sum_{k=0,1,2}\sqrt{2k+1}\begin{Bmatrix} L & \tilde{L} & \bar{L} \\ L' & \bar{L} & \tilde{L} \\ k & 1 & 1 \end{Bmatrix}$$

$$\times\sum_{mm'} t_{mm'}(-1)^{m'}\,C^{km-m'}_{1m1-m'}\,C^{LM_L}_{L'M'_Lkm-m}, \qquad [5]$$

where f is the phase ($f = n + 2S + \tilde{L} - \bar{L}$), $\begin{Bmatrix} \cdots \\ \cdots \\ \cdots \end{Bmatrix}$ is the 9–j-symbol, and $\langle \cdots \| \cdots \| \cdots \rangle$ is the reduced matrix element of the creation operator (42) that is to be calculated for each particular system.

Just as in spin systems, the matrix element of the double exchange contains the factor $(S + \frac{1}{2})$. The consequence is that double exchange in orbitally degenerate dimers always results in the stabilization of the ferromagnetic spin state, which, as for the spin MV dimers, becomes the ground state. This conclusion proves to be general for orbitally degenerate systems (irrespective of their structure and ground terms) and for spin systems. The matrix elements are independent of the quantum number M_S, indicating that the spin subsystem is magnetically isotropic.

The matrix elements of the double exchange for orbitally degenerate dimers depend on the orbital magnetic quantum numbers M_L, M'_L.This dependence reflects magnetic anisotropy in the orbital subsystem arising from the double exchange. The character of this anisotropy is closely related to the set of transfer integrals in Eq. [5], reflecting both the point symmetry of the dimer and the specific choice of physically significant transfer pathways. Therefore, a further analysis of the double-exchange energy splitting and the magnetic anisotropy requires a specific consideration for each particular case.

2.2. High–Symmetric Mixed–Valence Pairs

In this section we will consider three types of high-symmetric systems, namely, edge-shared (D_{2h}), corner-shared (D_{4h}), and face-shared (D_{3h}) bioctahedral dimeric clusters. Figure 2 pictorially represents the most important transfer pathways. In the case of D_{2h} symmetry we neglect all transfer integrals except $t_{\zeta\zeta}$ (Fig. 2a). In the case D_{4h} only the transfer integrals $t_{\xi\xi} = t_{\eta\eta}$ are taken into account (Fig. 2b). For the sake of simplicity we did not consider off-diagonal transfer pathways or less important diagonal ones (for example, $t_{\xi\xi}$ for D_{4h}). For D_{3h}, strong transfer between orbitals $a = (1/\sqrt{3})(\xi + \eta + \zeta)$ directed along the C_3 axis is taken into account (41, 43, 44) (Fig. 2c).

It follows from Eq. [5] for all these cases that $M'_L = M_L$, and the wave functions of the system can be expressed as an odd and even combination of the localized states:

$$|\pm SM_S; LM_L\rangle = \frac{1}{\sqrt{2}}(|\tilde{S}_A\tilde{L}_A, \bar{S}_B\bar{L}_B, SLM_SM_L\rangle \pm |\bar{S}_A\bar{L}_A, \tilde{S}_B\tilde{L}_B, SLM_SM_L\rangle). \quad [6]$$

It should be noted that there is no one-to-one correspondence between the parity of the wave functions and signs + and − in Eq. [6].

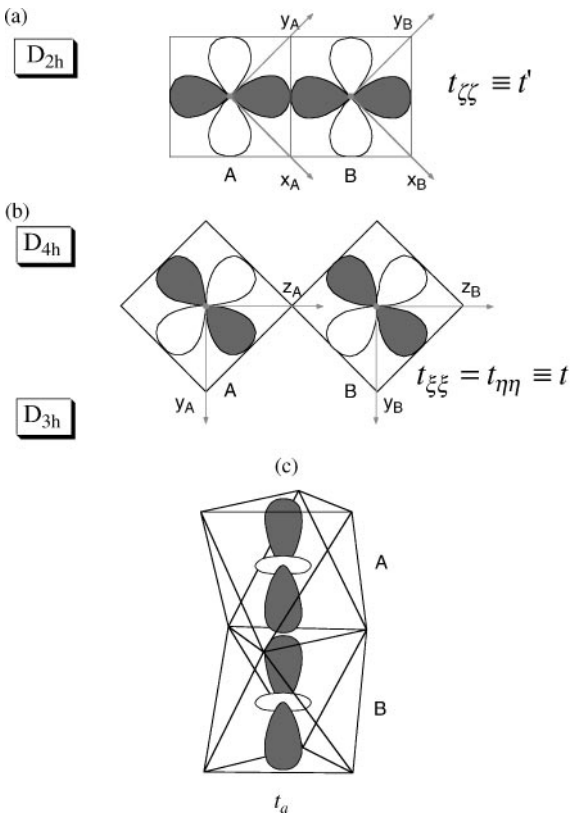

FIG. 2. The overlap patterns related to the most efficient transfer pathways: (a) D_{2h}, (b) D_{4h}, (c) D_{3h}.

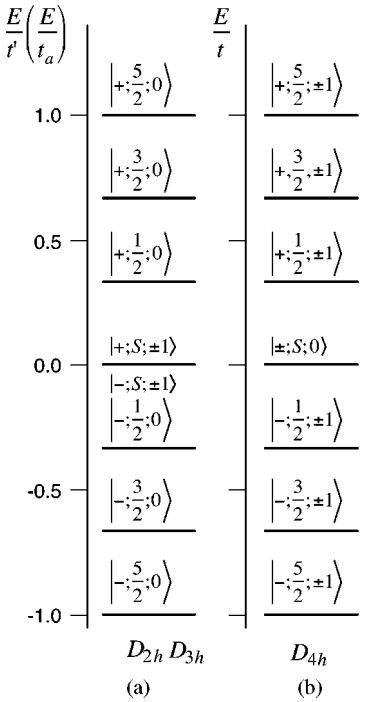

FIG. 3. Energy diagram for $^3T_1(t_2^2)$–$^4A_2(t_2^3)$ MV dimers: (a) D_{2h}, D_{3h}; and (b) D_{4h}. A short notation $|\pm; S, M_S; L = 1; M_L\rangle \equiv |S; M_L\rangle$ is used.

Since the spin system is isotropic, the quantum number M_S will be omitted, such that the labels will be $|\pm S; LM_L\rangle$. Let us first consider a singlet–triplet pair (one of the ions possesses orbital singlet). Figure 3 shows the energy splitting for a $^3T_1(t_2^2)$–$^4A_2(t_2^3)$ pair with different overall symmetries. Providing D_{2h} and D_{3h} symmetries (Fig. 3a), the energy pattern involves three pairs (+ and −) of levels with $S = \frac{1}{2}, \frac{3}{2}, \frac{5}{2}$; the corresponding energies are $\pm\frac{1}{3}t'(S + \frac{1}{2})$. All these levels correspond to $M_L = 0$. The spectrum also contains one highly degenerate level at $E = 0$. This level comprises states with all S values, each belonging to $M_L = \pm 1$.

In the case of D_{4h} symmetry (Fig. 3b) we encounter, in some sense, the reverse situation. Thus, the state with $E = 0$ involves all S values and corresponds to $M_L = 0$, while all the states with the energies $\pm\frac{1}{3}t(S + \frac{1}{2})$ possess $M_L = \pm 1$

The above analysis allows us to make some qualitative conclusions concerning the magnetic behavior. As we have seen, in all considered high-symmetric cases, the energy levels depend on $|M_L|$, so we are dealing with the axial magnetic symmetry. One should note in this context that for the D_{2h} system this axial symmetry is obviously higher than that expected from the point symmetry. This feature is a consequence of the simplified assumptions in the model of transfer pathways. The components of the magnetic susceptibility tensor ($\chi_\parallel$ and $\chi_\perp$) are defined with respect to the reference axis. For D_{4h} and D_{3h} systems this axis is chosen to coincide with the axis connecting the two metal sites (C_4

and C_3 axes, respectively). In the D_{2h} case this axis is perpendicular to the plane containing the common edge of the two octahedral sites (Z_A, Z_B C_2 axis in Fig. 2a). The spin part of the magnetic susceptibility is obviously isotropic and we must analyze the anisotropy arising from the orbital part $\Delta\chi = \chi_{\parallel}^{\mathrm{orb}} - \chi_{\perp}^{\mathrm{orb}}$.

The ground state for D_{2h} and D_{3h} dimers corresponds to $M_L = 0$; hence, in these cases $\chi_{\parallel}^{\mathrm{orb}} = 0$ at low temperature. $\chi_{\perp}^{\mathrm{orb}}$ appears as a second-order effect due to the mixture of the ground state with these excited states having the same spin and parity via a Zeeman term in a perpendicular field (nonvanishing matrix elements $\langle -; \frac{5}{2}, 0 | \mathbf{L}_x | -; \frac{5}{2}, \pm 1\rangle = \frac{1}{\sqrt{2}}$). Compared to the spin part, the orbital contribution to the susceptibility is expected to be small and the magnetic anisotropy, $\Delta\chi$, is negative in this case.

In the D_{4h} case, the situation is different because there is a strong first-order contribution to $\chi_{\parallel}^{\mathrm{orb}}$ arising from the $M_L = \pm 1$ ground state. This first-order orbital effect is strong and comparable with the spin part of susceptibility. The perpendicular Zeeman term mixes the ground state with the state $|-; \frac{5}{2}, 0\rangle$ giving rise to the second order $\chi_{\perp}^{\mathrm{orb}}$. As a result one can expect a magnetic anisotropy with a positive $\Delta\chi$.

Figure 4 represents the energy patterns for the triplet–triplet pair ${}^2T_2(t_2)$–${}^3T_1(t_2)$; the eigenvectors are given in Table 1. One can see that the energy levels are accidentally degenerate and the ground state for D_{2h}, D_{3h} contains a magnetic state with $L = 2$ and $|M| = 2$ giving rise to a first-order orbital Zeeman effect in parallel field ($\Delta\chi > 0$). One can see that the sign of $\Delta\chi$ in the system with a given overall symmetry for the triplet–triplet pair is reversed with respect to that for the singlet–triplet pair. In contrast, for the D_{4h} system the ground state is expected to possess a second-order magnetic effect, so that $\Delta\chi < 0$. As in the previous cases the triplet–triplet pair exhibits axial magnetic anisotropy.

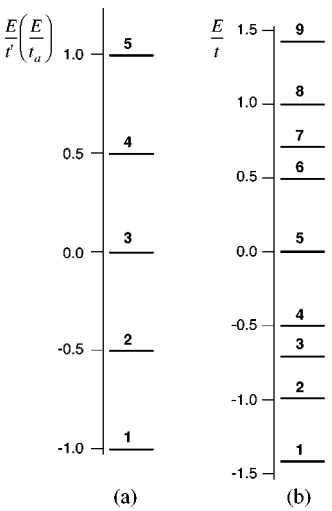

FIG. 4. Energy diagram for ${}^3T_1(t_2^2)$–${}^2T_2(t_2^1)$ MV dimers: (a) D_{2h}, D_{3h} cases and (b) D_{4h}. The eigenvectors are given in Table 1.

TABLE 1
Eigenvectors for the Dimer ${}^3T_1(t_2^2)$–${}^2T_2(t_2^1)$

Label of the level	D_{2h}, D_{3h}
(1)	$\lvert -;\frac{3}{2};1,0\rangle, \lvert +;\frac{3}{2};2,\pm 2\rangle, \frac{\sqrt{2}}{\sqrt{3}}\lvert -;\frac{3}{2};0,0\rangle + \frac{1}{\sqrt{3}}\lvert -;\frac{3}{2};2,0\rangle$
(2)	$\lvert -;\frac{1}{2};1,0\rangle, \lvert +;\frac{1}{2};2,\pm 2\rangle, \frac{\sqrt{2}}{\sqrt{3}}\lvert -;\frac{1}{2};0,0\rangle + \frac{1}{\sqrt{3}}\lvert -;\frac{1}{2};2,0\rangle$
(3)	$\lvert +;S;1,\pm 1\rangle, \lvert -;S;1,\pm 1\rangle, \lvert +;S;2,\pm 1\rangle, \lvert -;S;2,\pm 1\rangle, -\frac{1}{\sqrt{3}}\lvert -;S;0,0\rangle + \frac{\sqrt{2}}{\sqrt{3}}\lvert -;S;2,0\rangle, -\frac{1}{\sqrt{3}}\lvert +;S;0,0\rangle + \frac{\sqrt{2}}{\sqrt{3}}\lvert +;S;2,0\rangle$
(4)	$\lvert +;\frac{1}{2};1,0\rangle, \lvert -;\frac{1}{2};2,\pm 2\rangle, \frac{\sqrt{2}}{\sqrt{3}}\lvert +;\frac{1}{2};0,0\rangle + \frac{1}{\sqrt{3}}\lvert +;\frac{1}{2};2,0\rangle$
(5)	$\lvert +;\frac{3}{2};1,0\rangle, \lvert -;\frac{3}{2};2,\pm 2\rangle, \frac{\sqrt{2}}{\sqrt{3}}\lvert +;\frac{3}{2};0,0\rangle + \frac{1}{\sqrt{3}}\lvert +;\frac{3}{2};2,0\rangle$
Label of the level	**D_{4h}**
(1)	$\beta\lvert -;\frac{3}{2};0,0\rangle - \alpha\lvert -;\frac{3}{2};2,0\rangle, \alpha\lvert +;\frac{3}{2};0,0\rangle - \beta\lvert +;\frac{3}{2};2,0\rangle$
(2)	$\lvert -;\frac{3}{2};1,\pm 1\rangle, \lvert +;\frac{3}{2};2,\pm 1\rangle$
(3)	$\beta\lvert -;\frac{1}{2};0,0\rangle - \alpha\lvert -;\frac{1}{2};2,0\rangle, \alpha\lvert +;\frac{1}{2};0,0\rangle + \beta\lvert +;\frac{1}{2};2,0\rangle$
(4)	$\lvert -;\frac{1}{2};1,\pm 1\rangle, \lvert +;\frac{1}{2};2,\pm 1\rangle$
(5)	$\lvert \pm;S;1,0\rangle, \lvert +;S;2,\pm 2\rangle, \lvert -;S;2,\pm 2\rangle$
(6)	$\lvert +;\frac{1}{2};1,\pm 1\rangle, \lvert -;\frac{1}{2};2,\pm 1\rangle$
(7)	$\alpha\lvert -;\frac{1}{2};0,0\rangle + \beta\lvert +;\frac{1}{2};0,0\rangle, \beta\lvert +;\frac{1}{2};0,0\rangle - \alpha\lvert +;\frac{1}{2};2,0\rangle$
(8)	$\lvert +;\frac{3}{2};1,\pm 1\rangle, \lvert -;\frac{3}{2};2,\pm 1\rangle$
(9)	$\alpha\lvert -;\frac{3}{2};0,0\rangle + \beta\lvert +;\frac{3}{2};2,0\rangle, \beta\lvert +;\frac{3}{2};0,0\rangle - \alpha\lvert +;\frac{3}{2};2,0\rangle$

Note. The following notations are used: $\lvert \pm;S,M_S;L;M_L\rangle \equiv \lvert \pm;S;L;M_L\rangle$, $\alpha = \sqrt{\frac{1}{2} - \frac{\sqrt{2}}{3}}$, $\beta = \sqrt{\frac{1}{2} + \frac{\sqrt{2}}{3}}$.

Summarizing the results of this section we note that double exchange in orbitally degenerate systems produces ferromagnetic spin alignment and the same spin dependence of the energy levels as in spin systems. At the same time, the double exchange in the presence of orbital degeneracy results in a strong magnetic anisotropy of orbital nature. For this reason, it can be termed as *anisotropic double exchange*. The character of the magnetic anisotropy in a MV pair is closely related to the ground terms of the constituent ions, transfer pathways, and overall symmetry of the system. It should also be noted that this qualitative analysis of the magnetic anisotropy proved to be possible due to the use of a pseudoangular momentum representation attributing to the system a set of relevant quantum numbers.

2.3. *Influence of the Vibronic Coupling on the Magnetic Anisotropy*

The vibronic interaction in MV compounds is usually important so that manifestations of the mixed valency are closely related to the strength of the vibronic coupling. In order to illustrate (at least at the qualitative level) the main

effects of the vibronic coupling we will use a vibronic model that assumes the local breathing modes (PKS, (45)) but that includes also the intercenter vibrations changing the metal–metal distance (46). Such a type of vibronic model was used in our paper (47) to study the adiabatic potentials and localization–delocalization effects in spin-dimers. Remaining within the scope of this simplified model we do not intend to discuss here the applicability of the theory operating with two vibronically independent subunits (see Ref. (45)). We also omit from our discussion the role of the local Jahn–Teller vibrations. This problem will be discussed elsewhere.

In order to inspect the role of the vibronic effects in the context of the magnetic properties we will restrict ourselves to the simplest case of the singlet–triplet pair (considered in Section 2.1). Let us denote the coordinate of the out-of-phase PKS vibration as q and that for the intercenter vibration as Q. The PKS interaction mixes the states with the same quantum numbers S, M_S, M_L and opposite parity, thus leading to the pseudo-Jahn–Teller effect. On the other hand, the interaction with the Q mode is diagonal in the $|p, S; M_L\rangle$ basis. In fact, this interaction leads to a modulation of the transfer integrals t and t' due to the changes of the intermetallic distances (see (46, 48)). The S, M_L block of the adiabatic potentials involving the interactions with the dimensionless q and Q vibrations can be presented as (49):

$$D_{2h}: U_{\pm}^{S;M_L}(q, Q) = \tfrac{1}{2}(\omega q^2 + \Omega Q^2) \pm \left[\frac{1}{9}(t - \lambda Q)^2 (1 - |M_L|(S + \tfrac{1}{2})^2 + \tfrac{1}{2} v^2 q^2\right]^2$$

$$D_{4h}: U_{\pm}^{S;M_L}(q, Q) = \tfrac{1}{2}(\omega q^2 + \Omega Q^2) \pm \left[\frac{1}{9}(t - \lambda Q)^2 (|M_L|)(S + \tfrac{1}{2})^2 + \tfrac{1}{2} v^2 q^2\right]^2, \qquad [7]$$

where ω and Ω are the frequences of the q and Q modes, respectively, and λ and v are the coupling parameters for the intercenter and PKS vibrations. For both topologies under consideration the energy pattern contains the unsplit level $\varepsilon = 0$ comprising all S states with $M_L = \pm 1$ for D_{2h} and $M_L = 0$ for D_{4h}. These levels give rise to the intersected paraboloids shifted along the q axis toward the points $\pm(\vartheta/\omega\sqrt{2})$ $(Q = 0)$. The remaining surfaces belong to definite S values and their shapes are quite similar to those studied in detail in the problem of double exchange (47). Let us summarize the main features of these adiabatic surfaces responsible for the magnetic behavior of the system.

Providing strong PKS coupling, $\vartheta^2/2\omega > \lambda^2/9\Omega(S + \frac{1}{2})^2$, and comparatively weak transfer, $t/3(S + \frac{1}{2}) < \vartheta^2/2\omega - \lambda^2/9\Omega(S + \frac{1}{2})^2$, we are dealing with a double-well surface so that in each minimum the excess electron is localized. In the case of strong PKS coupling and strong transfer $t/3\ (S + \frac{1}{2}) > \vartheta^2/2\omega - \lambda^2 9\Omega(S + \frac{1}{2})^2$, the surface possesses a single minimum with shifted Q and the excess electron is fully delocalized. Finally, in the case of weak PKS coupling, $\vartheta^2/2\omega < \lambda^2/9\Omega(S + \frac{1}{2})^2$, the system is fully delocalized independently of the rate of transfer.

Let us consider the influence of breathing and intermetallic vibrations separately. Figure 5 represents the section $Q = 0$ of the full adiabatic surface for $S = \frac{5}{2}$ of the singlet–triplet pair in the D_{4h} case (these levels are extracted from the full set of levels depicted in Fig. 3b). Due to the preference in the Jahn–Teller stabilization of the $M = 0$ central level with respect to those for $M = \pm 1$, the gap $2t$ between the levels $|+; \frac{5}{2}; \pm 1\rangle$ and $|-; \frac{5}{2}; \pm 1\rangle$ proved to be compressed in the deep minima. The resulting levels in these minima contain all sublevels $M_L = 0, \pm 1$ belonging to $L = 1$, and of course $S = \frac{5}{2}$ (^6P atomic level). In this way we arrive at the conclusion that the vibronic PKS coupling suppresses the magnetic anisotropy of the system.

Figure 6 illustrates the section $q = 0$ of the adiabatic surface for the selected $S = \frac{5}{2}$ spin state. One can see that the intercenter vibration stabilizes the ground state with $M_L = 1$ with respect to that with $M_L = 0$. In fact, in the deep minimum associated with $M_L = \pm 1$ the corresponding gap $\Delta E_{\min}$ is strongly increased with respect to the initial $(Q = 0)$ gap, t, produced by the double exchange. This can be considered as an increase in the anisotropy. This is not a surprising result because the intercenter vibration effectively

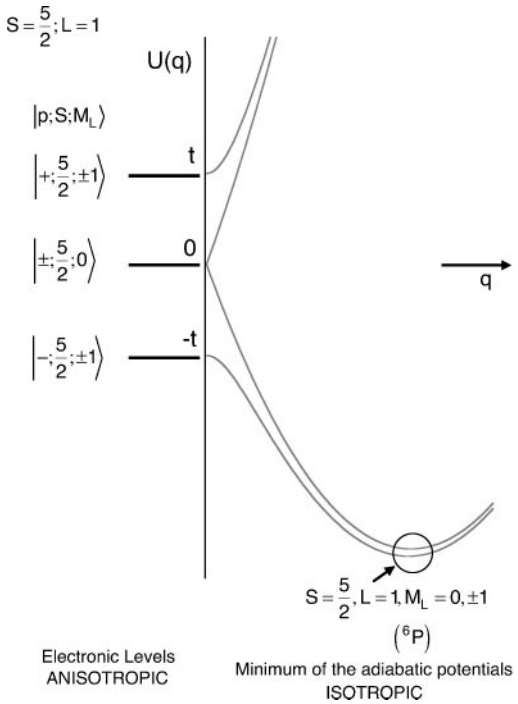

FIG. 5. Suppression of the magnetic anisotropy by PKS vibration as illustrated by the singlet–triplet pair in the D_{4h} system.

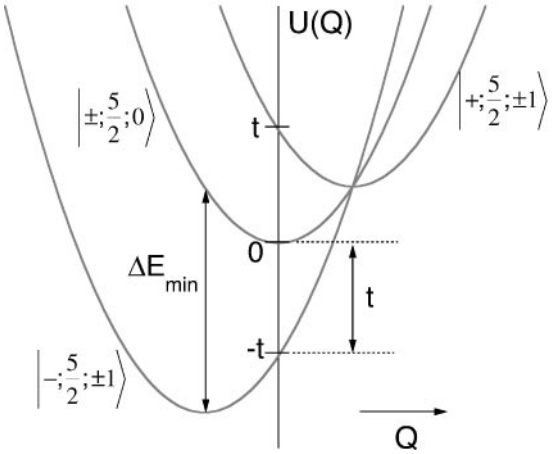

FIG. 6. Enhancing the magnetic anisotropy by the intercenter vibration Q, as illustrated by a singlet–triplet pair in D_{4h} symmetry.

increases the double exchange that is the origin of the magnetic anisotropy in the case of degeneracy.

We have considered in a qualitative manner the effects of two kinds of vibrations independently by crossing the three-dimensional adiabatic surface $U(q, Q)$ in two directions. At the same time (as already mentioned in (47)) the breathing and intercenter vibrations are competitive. The conditions for the existence of localized (strong PKS coupling) or delocalized (strong coupling with the intercenter vibration) are spin-dependent. In Fig. 7 we present the picture of the adiabatic surfaces belonging to several spin states of the singlet-triplet pair in D_{4h} symmetry.

Figure 7 illustrates the case when the low branch of the full adiabatic surface $U_-(q, Q)$ has delocalized minima only for the $S = \frac{5}{2}$ states. Due to the large gap between two $S = \frac{5}{2}$ levels, PKS coupling is reduced and the system proves to be trapped in this delocalized state. At the same time for $S = \frac{3}{2}$ and $S = \frac{1}{2}$ pairs we observe two minima (intercenter coupling is reduced) in which the system is partially localized due to the coupling with PKS vibrations. In the present case the used values of the vibronic parameters ($t = 1.0$, $v = 2.5$, $\lambda = 1$) favor an increase in the magnetic anisotropy due to the stabilization of the $M_L =$ state. The calculation of $\chi_\parallel$ and $\chi_\perp$ for the anisotropic double exchange systems is given in (49).

3. MAGNETIC EXCHANGE IN THE CASE OF DEGENERACY

3.1. *Effective Hamiltonian of the Magnetic Exchange*

A new approach to the problem of the magnetic exchange for orbitally degenerate ions was recently developed in our laboratories (40, 41). In these studies, the constituent multielectron ions were assumed to be octahedrally coordinated, and a strong cubic crystal field scheme was employed, enabling us to take advantage of the symmetry properties of the fermionic creation and annihilation operators and multielectron wave functions of the metal ions. In the framework of this microscopic approach, the effective Hamiltonian of the kinetic exchange was built. As distinguished from the previous studies, this Hamiltonian was derived for the general case of multielectron ions and arbitrary topology of the system implied by a set of the electron transfer parameters. The Hamiltonian was constructed in terms of spin operators and orbital cubic irreducible tensor operators acting in the orbital subspace.

Along with the isotropic spin–spin exchange (HDVV term) this Hamiltonian includes terms like $\mathbf{O}_{\Gamma_A\gamma_A}\mathbf{O}_{\Gamma_B\gamma_B}\,\mathbf{S}_A\mathbf{S}_B$ where $\mathbf{O}_{\Gamma_A\gamma_A}$ and $\mathbf{O}_{\Gamma_B\gamma_B}$ are the orbital matrices defined in the space of the orbitally degenerate functions belonging to the constituent ions. The labels Γ_A and Γ_B are the irreducible representations contained in a direct product $\Gamma\times\Gamma$, with ${}^{2S+1}\Gamma$ being the ground term. $\gamma_{A(B)}$ are labels for the basis. For example, for the orbital triplets T_2, $T_2\times T_2 = A_1 + E + T_1 + T_2$ and we have nine matrices $\mathbf{O}_{\Gamma_{A(B)}\gamma_{A(B)}}$. These 3×3 matrices are given in (41). Here we want only to stress that in general they do not commute with $\hat{L}^2$ and L_z, so the full Hamiltonian containing these matrices is magnetically anisotropic.

In paper (50) we suggested the use of a pseudoangular representation for the orbital triplets ($L = 1$ for T_1 and

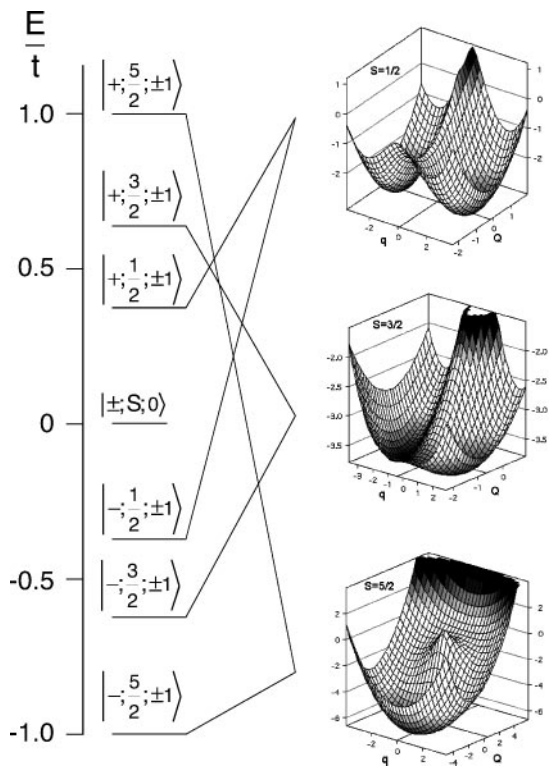

FIG. 7. Adiabatic surfaces for selected spin states of a singlet–triplet MV pair in D_{4h} ($t = 1$, $v = 2.5$, $\lambda = 1$); all values are given in $\Omega = \omega$ units).

T_2 terms) and the technique of the irreducible tensor operator in a spherical group (ITO) for treating the Hamiltonian containing orbital matrices. This approach provides an efficient way for the calculating the energy levels and allows us to label them in terms of spin and atomic orbital quantum numbers using the Russell–Saunders coupling scheme for the pseudoangular orbital momenta. This approach is quite similar to that described in Section 2 for MV systems. In the following subsection we will illustrate the results of the application of this approach to analyze the magnetic anisotropy of high-symmetric systems.

3.2. *Corner–Shared* (D_{4h}) d^1–d^1 *Dimers*

We will illustrate the results taking as an example the simple case of d^1 ions ($^2T_2$–$^2T_2$ system) for which all parameters of the orbitally dependent exchange Hamiltonian are calculated analytically (40).

The $t_{\xi\xi} = t_{\eta\eta} \equiv t$ transfer integrals (Fig. 2) are taken into account, and the crystal field and Racah parameters are given in (51). In paper (50) we considered the exchange Hamiltonian using ITO; the local crystal fields (C_{4v}) and the spin–orbit coupling as well as the Coulomb repulsion between unfilled shells, were also taken into account. The energy pattern arising from the exchange is given in Fig. 8, where the labels of the irreducible representations of D_{4h} are given along with the labels $|SM_S; LM_L\rangle \equiv |S; L\, M_L\rangle$. The ground state **1** proves to be a spin triplet belonging to $L = 1$, $M_L = 0$ so that at low temperature only a small magnetic spin anisotropy could be expected. The next two levels (**2** and **3**) are the spin singlets corresponding to $L = 2$. These states are $(|0; 2\ -2\rangle \pm |0; 2\ 2\rangle)/\sqrt{2}$. Each one of these states is orbitally nonmagnetic (all matrix elements of $\mathbf{L}_z$, $\mathbf{L}_x$ and $\mathbf{L}_y$ vanish). Nevertheless, it should be noted that levels **2** and **3** are very close, due to the fact that the ^1E and $^1T_2$ charge-transfer states are almost degenerate (see the Tanabe–Sugano diagram for d^2 (51) and the discussion concerning the exchange parameters in Ref. (40)). In fact for the set of crystal field parameters (D_q, A, B, and C) used here the gap ΔE_{23} proves to be equal to 0.02 cm^{-1} (this gap is artificially increased in Figs. 8 and 9), which is much less than Zeeman energy ($\approx 0.1 - 1\ cm^{-1}$). Under these conditions these two levels are fully mixed, giving rise to a first-order orbital magnetic splitting when the field is applied parallel to the C_4 axis (the functions are $|0; 2 \pm 2\rangle$). At the same time, the first-order perpendicular magnetization vanishes and appears only as a second-order effect. Hence, the orbital contribution to the magnetic susceptibility is fully anisotropic. Levels **5** and **6** show a first-order contribution to the orbital magnetic moment along the C_4 axis but no first-order contribution in the perpendicular field. Finally, the same conclusion can be drawn about the accidentally degenerate level **7**, comprising two spin singlets and four spin triplets. One can see also that all matrix elements $\langle 1; 1\ 0|\hat{L}_z|$ excited states$\rangle$ vanish, so that one cannot expect the second-order orbital contribution in $\chi_\parallel^{orb}$. Nonvanishing orbital contribution may appear only due to the spin–orbit mixing of the ground state $|1; 1\ 0\rangle$ with the excited ones (levels **5** and **6**). At the same time the matrix element $\langle 1; 1\ 0|\hat{L}_{x,y}|1; 1 \pm 1\rangle$ is different from 0. This gives rise to a second-order contribution to $\chi_\perp^{orb}$. Therefore, at low temperature, it is expected that $\chi_\perp^{orb} > \chi_\parallel^{orb}$. With the increase of temperature levels **2** and **3** become populated, giving rise to a first-order effect with strong $\chi_\parallel^{orb}$ and small second-order $\chi_\perp^{orb}$, the last results from the mixing of levels **2** and **3** with level **6** ($|0; 2 \pm 1\rangle$). Summarizing, one can conclude that the exchange Hamiltonian for the $^2T_2$–$^2T_2$ pair is completely anisotropic in the sense that $\chi_\parallel^{orb}$ appears as a first-order effect, meanwhile $\chi_\perp^{orb}$ proves to be a second-order effect.

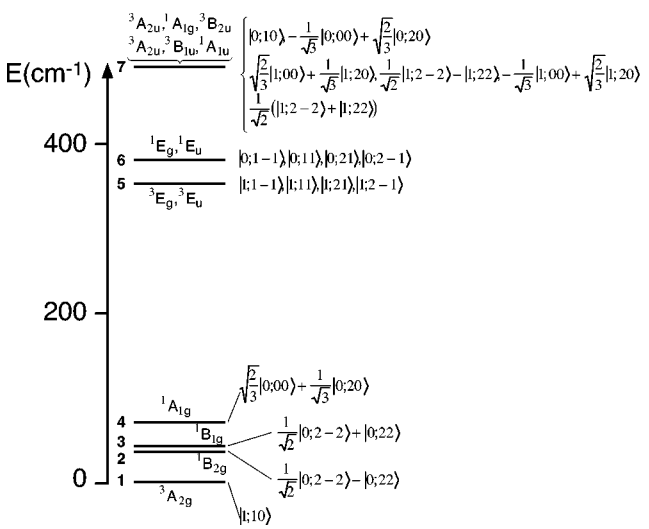

FIG. 8. Exchange splitting in the corner–shared (D_{4h}) cluster consisting of one-electron ions $|\pm; S, M_S; L, M_L\rangle \equiv |\pm; S; L, M_L\rangle$.

Figure 9 shows the influence of the tetragonal crystal field distortion with $\Delta > 0$ (ground state of each ion is $B_2(\zeta)$). The increase of Δ changes the ground state $|1; 1\ 0\rangle$ into the paramagnetic mixture of spin–triplet and spin–singlet states as shown in Fig. 9. These two states arise from the ground states ζ_A and ζ_B as a result of the strong crystal field splitting. Since in the initial model weak $\zeta_A \leftrightarrow \zeta_B$ transfer has been neglected, the exchange effect in the ground manifold vanishes. As one can see, both states possess $M_L = 0$ so that first-order $\chi_\perp^{orb} = \chi_\parallel^{orb} = 0$ and second-order effect in $\chi_\perp^{orb}$ decreases with the increase of crystal field. If a small $\zeta_A \leftrightarrow \zeta_B$ transfer is assumed, the ground level is split antiferromagnetically as one would expect for a dimer with two half-occupied orbitals (this is schematically shown by the dotted line in Fig. 9). In the low-temperature limit, the full magnetic susceptibility only contains the orbital part with $\chi_\perp^{orb}$ being a second-order effect and $\chi_\parallel^{orb} = 0$. Second-order

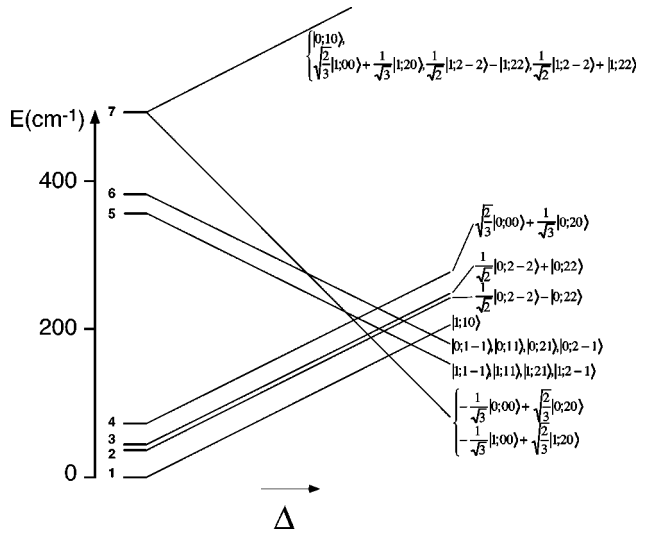

FIG. 9. Effect of local tetragonal crystal field on the energy pattern of the $^2T_2$–$^2T_2$ dimer (D_{4h}).

$\chi_\perp^{orb}$ (Van Vleck paramagnetism) can be easily estimated. In fact, the orbital part of Zeeman interaction mixes the ground state $(-|0;0\ 0\rangle+\sqrt{2}|0;2\ 0\rangle)/\sqrt{3})$ only with the states $|0;2\pm1\rangle$ belonging to the multiplet 6; the corresponding matrix elements are

$$\langle 0;0\ 0|\hat{L}_x|0;2\pm1\rangle = 0$$

$$\langle 0;2\ 0|\hat{L}|0;2\pm1\rangle = \sqrt{\tfrac{3}{2}}. \qquad [8]$$

One can easily obtain the second-order Zeeman coefficient and find $\chi_\perp$

$$\chi_\perp(T=0) = \frac{4N\beta^2k^2}{E_6 - E_7 + 3\Delta}, \qquad [9]$$

where k is the orbital reduction factor. Due to the spin–orbit mixing of the ground state with the excited ones a $\chi_\parallel$ contribution appears, but this is small if the crystal field splitting is strong enough so that $\chi_\perp > \chi_\parallel$. This conclusion illustrates that the low-symmetry crystal field can reverse the sign of the orbital part of the magnetic anisotropy arising from the orbitally dependent exchange interaction.

This analysis once again illustrates that the angular momentum approach is not only an efficient computational tool, but is also of great help in the understanding of the magnetic properties (especially the magnetic anisotropy).

3.3. *Face-Shared* (D_{3h}) d^1–d^1 *Dimers. Magnetic Anisotropy of* $[Ti_2Cl_9]^{-3}$

In the present section, we apply the effective Hamiltonian deduced in (41) to the case of the face-shared bioctahedral $d^1(^2T_2)$–$d^1(^2T_2)$ dimer (with overall D_{3h} symmetry). Trivalent titanium ions form this type of well isolated dimer in the crystal structure of $Cs_3Ti_2Cl_9$ (35, 52) and $Cs_3Ti_2Br_9$ (34) whose magnetic and spectroscopic properties were a subject of the discussion for a long time (31, 36, 39, 43, 44, 53). The full effective Hamiltonian for a face-shared dimer was deduced in paper (41). The t_a (Fig. 2) and t_e transfer integrals were taken into account (t_e are formed by e-orbitals that are perpendicular to C_3 axis in D_{3h}) (43).

In the previous section we have restricted the consideration by the most efficient transfer pathways only. In order to study the dependence of the degree of anisotropy upon the transfer integrals we have included both types of integrals, t_a and t_e, in the calculation. Figure 10 shows the calculated energy levels as a function of the ratio t_e/t_a in the range $-1 \le t_e/t_a \le 1$. One can see that the energy pattern is symmetric with respect to the change of the sign of t_e/t_a. In a wide range of the ratio t_e/t_a, the ground state is the spin singlet $^1A_1'$. Only at $t_e/t_a > 0.9$ ($t_e/t_a < -0.9$) does the orbital doublet $^3E'$ ($^3E''$) become the ground state. The highest excited state is accidentally degenerate and comprises several multiplets, mainly spin triplets. It is to be noted that, except in the extremes of the diagram, the exchange splitting (except terminal parts of the diagram) is almost independent of the ratio t_e/t_a and mainly depends on t_a.

Three special high-symmetric cases are seen in Fig. 10, namely:

(i) Pseudospherical case: $t_e/t_a = 1$ ($t_a = t_e = t, t' = 0$),
(ii) Spherical case: $t_e/t_a = -1$ ($t = -t_a/3, t' = -2t$),
(iii) Axial case: $t_e/t_a = 0$ ($t = t' = t_a/3$).

In each of these cases, the energy pattern exhibits a high degree of accidental degeneracy, a clear indication that the effective Hamiltonian belongs to a more general symmetry

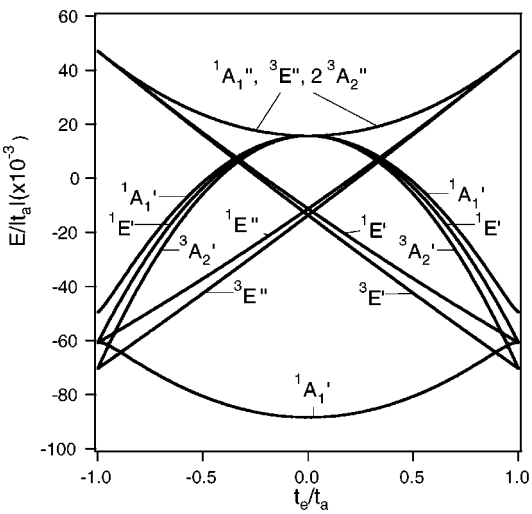

FIG. 10. Energy pattern of the face-shared $^2T_2$–$^2T_2$ system as a function of t_a/t_e.

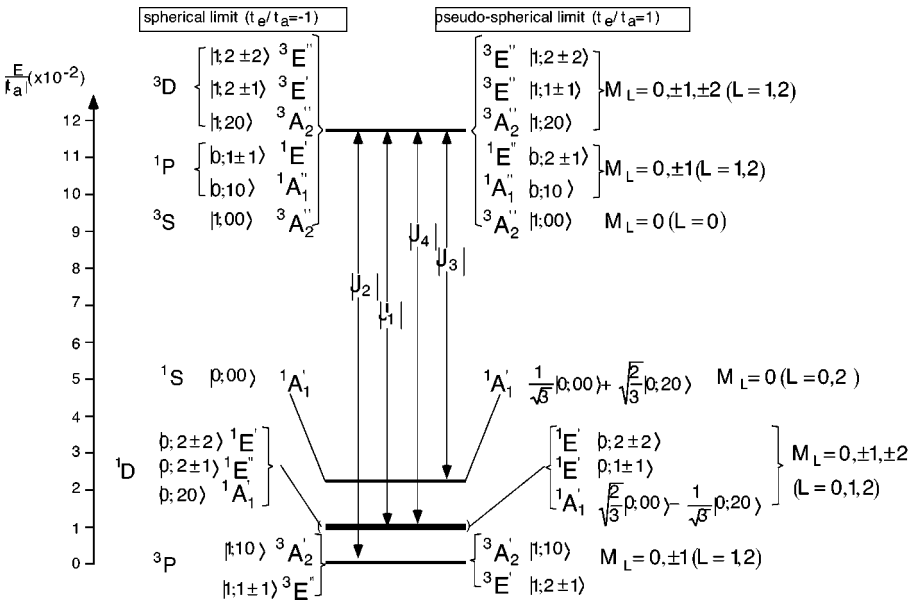

FIG. 11. Energy pattern of the face-shared $^2T_2$–$^2T_2$ system in the spherical (left-side labels) and pseudospherical (right-side labels) limits.

group than the point symmetry group D_{3h}. The terms pseudospherical, spherical, and axial are closely related to the magnetic anisotropy and will be clarified below.

Let us consider first the cases (i) and (ii). Since the diagram is symmetric, the energy patterns for spherical and pseudospherical limits are the same. This is depicted in Fig. 11, where the terms for cases (i) and (ii) are shown on the right and left sides correspondingly. The exchange parameters $J_1 \cdots J_4$ are given in (41).

As in the previous cases, the Hamiltonian, expressed in terms of the ITO, acts within the basis set $|L_A L_B S_A S_B, SM_S LM_L\rangle \equiv |SM_S, LM_L\rangle$ with fictitious $L_A = L_B = 1$ and $L = 0, 1, 2$ (Russell–Saunders coupling scheme).

Let us start with the pseudospherical case (i). The ground level comprises two terms, $^3A_2'$ and $^3E'$, that can be associated with $|1; 10\rangle$ and $|1; 2 \pm 1\rangle$ functions. Let us consider the anisotropy coming from the orbital contributions. One can see that $|1; 2 \pm 1\rangle$ states lend a strong orbital contribution to $\chi_\parallel$, meanwhile the matrix elements of L_x and L_y disappear within the ground manifold ($L = 1$ for $^3A_2'$ and $L = 2$ for $^3E'$). Inspecting all $|S; LM_L\rangle$ labels one can see that the operator L_z has nonvanishing matrix elements within all levels with $M_L \neq 0$ ($L = 1, 2$). In contrast, the matrix elements of L_x and L_y vanish within each exactly and accidentally degenerate level in Fig. 11. The matrix elements of these operators also vanish within the basis belonging to six low-lying levels. The nonvanishing matrix elements link only the low-lying states with the highest group of states. For these reasons, the perpendicular component of the orbital part of the magnetic susceptibility appears as the second-order effect. Hence one can expect that $\chi_\parallel > \chi_\perp$, so the magnetic anisotropy defined as $\Delta\chi = \chi_\parallel - \chi_\perp$ proves to be positive.

Finally we would like to underscore the point that each level in case (i) is $(2M_L + 1)$-fold degenerate (like in a spherically symmetric system) but does not correspond to a definite value of $L = M_{L_{\max}}$ (for example, $L = 1$ and $L = 2$ in the ground state with $M_L = -1, 0, 1$) as indicated in Fig. 11. For this reason we refer to this case as the pseudospherical (but not spherical) limit. Indeed, from the point of view of magnetic anisotropy discussed thus far, this case should be referred to as completely anisotropic. It is to be noted that the pseudospherical limit occurs under the *spherical* condition $t_a = t_e$ for the transfer integrals.

Next let us consider now the spherical case (ii). The energy levels are the same as in the previous case (Fig. 10), but the wave functions are different (see labels in the left part of Fig. 11). The general feature of this energy pattern is that each level can be associated with one or several atomic terms SL as shown in Fig. 11. In fact, the ground state containing accidentally degenerate levels $^3A_2'(|1; 10\rangle)$, $^3E''(|1; 1, \pm 1\rangle)$ can be regarded as an atomic term with $L = 1$ and $S = 1$ (^3P); the first excited state possesses $L = 2$ and $S = 0$ (^1D), etc. This shows that, unlike the previous case, the system in the limit $t_a/t_e = -1$ is magnetically isotropic. Therefore this case can be referred to as the true spherical limit.

The last case we consider here is the axial limit ($t_e = 0$). In this case the ground state is the orbital and spin singlet state $^1A_1'$ (which corresponds to the wave function $-\frac{1}{\sqrt{3}}|0; 00\rangle + \sqrt{\frac{2}{3}}|0; 20\rangle$ fin pseudo-angular momentum representation. The first excited group of levels consists of two closely spaced sublevels. One of them (lower) comprises

spin triplets $^3E'$, $^3E''$, and another spin singlets $^1E'$, $^1E''$. Finally, the highest level comprises both spin triplets and spin singlets. Since $M_L = 0$ and $S = 0$ in the ground state, $\chi_\parallel = 0$ in the low temperature limit. At the same time, $\chi_\perp$ appears as a second-order effect (temperature-independent Van–Vleck paramagnetism) due to the mixing of the ground state with the excited states $|0; 2 \pm 1\rangle$ ($^1E''$) through the orbital part of Zeeman interaction. The anisotropy $\Delta\chi$ proves to be negative, i.e., it has the reverse sign with respect to the pseudospherical case.

This conclusion about negative magnetic anisotropy is valid also for the range of t_e/t_a (Fig. 10) in which the ground term is $^1A_1$ (superposition of $|0; 00\rangle$ and $|0; 20\rangle$). When $^3E''$ ($t_e/t_a < -0.9$) or $^3E'$ ($t_e/t_a > 0.9$) are the ground terms ($M_L = \pm 1$), $\Delta\chi$ is positive. In all cases (with the exception of the true spherical limit $t_e/t_a = -1$) the magnetic anisotropy is axial ($|M_L|$ is a good quantum number) and $\Delta\chi$ dependson the ratio t_e/t_a.

The correlation diagram in Fig. 12 illustrates how the pattern of the energy levels formed by the orbitally dependent exchange interaction in the $^2T_2 - {}^2T_2$-pair in the pseudo spherical limit is modified under the influence of the trigonal crystal field provided $\Delta < 0$ (orbital singlet $^2A_1$ in the ground state of each ion). As one can see from Fig. 12, the trigonal field partially removes the accidental degeneracy of the exchange multiplets contributing anti ferromagnetically to the low-lying group of levels. The increase of the absolute value of the trigonal field parameter $|\Delta|$ leads to the crossing of the spin levels $^1A'_1$ and $^3E'$ so that the system becomes antiferromagnetic, even for a very weak trigonal field. In the limit of a strong trigonal field, the low-lying

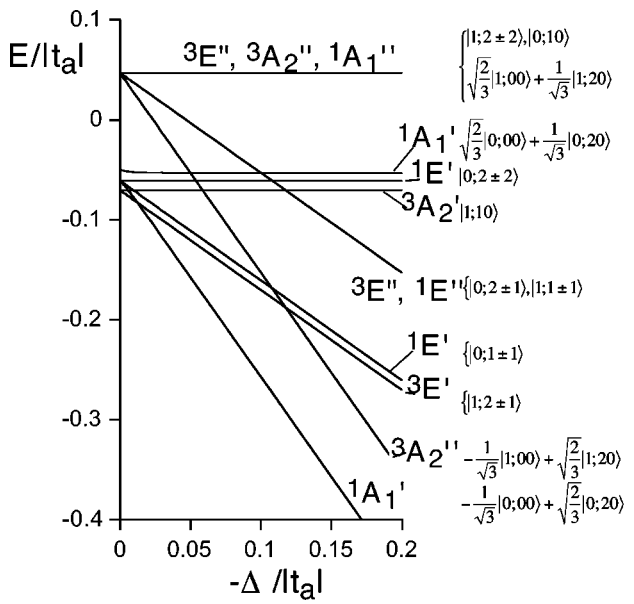

FIG. 12. Influence of the local trigonal field ($\Delta < 0$) on the energy pattern of the ^2T–^2T face-shared system in the pseudospherical limit.

group of levels proves to be well isolated and consists of the orbitally nondegenerate spin singlet $^1A'_1$ (ground) and the spin triplet $^3A''_2$; the energy separation between them is found to be $\varepsilon\,(^3A''_2) - \varepsilon(^1A'_1) = -(J_1 + J_3)$. This pair of levels can be described by the isotropic HDVV Hamiltonian $-2J_{\text{eff}}\mathbf{S}_A\mathbf{S}_B$ with $J_{\text{eff}} = \frac{1}{2}(J_1 + J_3)$. The exchange interaction proves to be antiferromagnetic.

Concerning the influence of the trigonal field on the magnetic behavior, two points should be mentioned. First, the trigonal field should strongly reduce the magnetic susceptibility because of the stabilization of the state $^1A'_1$ that carries neither spin nor orbital magnetic moment. Second, the trigonal field tends to change the sign of the anisotropy. At the low temperatures $\chi_\parallel$ tends to 0, meanwhile $\chi_\perp$ tends to the nonzero value due to a second-order Zeeman effect. In fact, inspecting the $S; LM_L$ labels in Fig. 12 one can see that the ground state $^1A'_1$ $(-\frac{1}{\sqrt{3}}|0; 00\rangle + \sqrt{\frac{2}{3}}|0; 20\rangle)$ can mix through $L_\perp$ with the state $^1E''$ ($|0; 2 \pm 1\rangle$), whereas L_z cannot mix the ground state with the excited states. With the further increase of $|\Delta|$ the second–order effect decreases and the system becomes more isotropic.

In order to restrict the number of the adjustable parameters in the fitting of the experimental data we will use the ratio of two transfer integrals t_a and t_e extracted from the *ab initio* calculations of Ceulemans *et al.* (44). They roughly estimated this ratio as $t_a/t_e \approx -6.5$ (-7 in Refs. (43, 53)).

In the best fit procedure we use the same values for the crystal field and Racah parameters as in Section 3, $\lambda = 155\ \text{cm}^{-1}$, and vary t_a, Δ, and k. Figure 13 displays the experimental temperature dependencies of $\chi_\parallel$ and $\chi_\perp$ for $Cs_3Ti_2Cl_9$ obtained by Briat *et al.* (35) and the theoretical curves. The best fit is achieved for $t_a = -5208\ \text{cm}^{-1}$, $\Delta = -320\ \text{cm}^{-1}$, and $k = 0.71$. One can see that the theoretical curve for $\chi_\perp$ is in excellent agreement with the experimental data in the low-temperature region (below 170 K). The calculated $\chi_\parallel$ at low temperature is in satisfactory agreement with the experimental values. It is also remarkable that the theory reproduces the slopes of $\chi_\parallel$ and $\chi_\perp$ very well. It should be emphasized that nonvanishing $\chi_\parallel$ appears only due to allowance for the spin–orbital interaction. Another important feature of the magnetic behavior of $Cs_3Ti_2Cl_9$ is the temperature dependence of the magnetic anisotropy. Figure 13 (inset) shows that, in a good agreement with the experimental data, $\Delta\chi_{\text{theor}}$ remains constant below 100 K and decreases with the increase of T at $T > 150$ K.

4. CONCLUDING REMARKS

In this paper we have attempted to analyze some consequences of the orbital degeneracy in highly symmetric dinuclear systems. We have considered delocalized (mixed-valence) and localized (exchange) systems. The use of the concept of an orbitally dependent exchange Hamiltonian

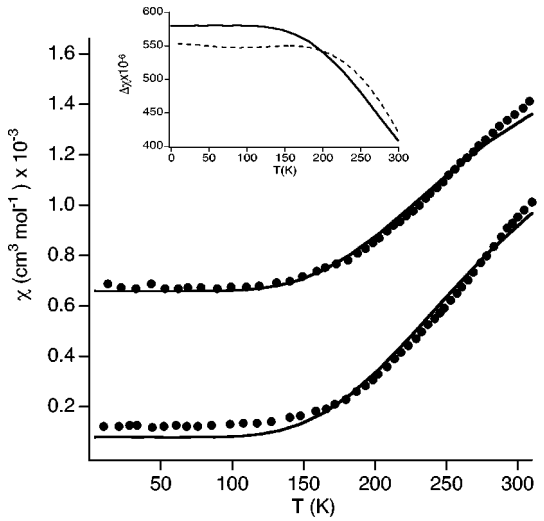

FIG. 13. Magnetic behavior of the $[Ti_2Cl_9]^{-3}$ unit: comparison with the theoretical curve (solid line) calculated at $t_e/t_a = -0.154$, $t_a = -52028\ cm^{-1}$, $\Delta = -320\ cm^{-1}$, $\lambda = 155\ cm^{-1}$ and orbital reduction function $k = 0.71$. (Inset) Temperature dependence of the degree of anisotropy, compared with the theoretical curve (solid line).

and pseudoangular momentum representation (based on the technique of ITO) allowed for the calculation of the energy pattern of MV and exchange clusters and to assign to the energy levels the labels of angular orbital momenta. This provides clear insight into the magnetic anisotropy of the systems arising from the orbital interactions. The main manifestation of the orbitally dependent exchange and *anisotropic double exchange* is the appearance of a strong magnetic anisotropy in the system. The energy pattern and the character of the anisotropy are specific for each kind of MV or exchange coupled pair. They are closely related to the ground states of the constituent ions, transfer pathways, and overall symmetry of the system. The vibronic interaction with breathing modes in mixed-valence systems suppresses the magnetic anisotropy, while the coupling with the intercenter vibration increases the magnetic anisotropy.

ACKNOWLEDGMENTS

Financial support of the European Union (Network on Molecules as Nanomagnets, HPRN–CT–1999–00012), the Ministerio de Ciencia y Tecnología (Grant MAT98–0880) and the Generalitat Valenciana (Grant GVDOC00–01–02) are acknowledged. B.S.T. thanks the Universidad de Valencia and the European Science Foundation for a Visiting Professor grant (Programme of *Molecular Magnets*). J.M.C.J. thanks also the MEC for a post-doctoral fellowship.

REFERENCES

1. D. Gatteschi, A. Caneschi, L. Pardi, and R. Sessoli, *Science* **265,** 1054 (1994).
2. R. Sessoli, D. Gatteschi, A. Caneschi, and M. A. Novak, *Nature* **365,** 141 (1993).
3. M. R. Cheesman, V. S. Oganesyan, R. Sessoli, D. Gatteschi, and A. J. Thomson, *Chem. Commun.* 1677 (1997).
4. G. J. Eppley, H. L. Tsai, N. de Vries, G. Christou, and D. N. Hendrickson, *J. Am. Chem. Soc.* **117,** 301 (1995).
5. R. Sessoli, H. L. Tsai, A. R. Schake, S. Wang, J. B. Vincent, K. Floting, D. Gatteschi, G. Christou, and D. N. Hendrickson, *J. Am. Chem. Soc.* **115,** 1804 (1993).
6. S. M. J. Aubin, Z. Sun, I. A. Guzei, A. L. Rheingold, G. Christou, and D. N. Hendrickson, *Chem. Commun.* 2239 (1997).
7. I. Fujita, Y. Yeki, T. Takui, T. Kinoshita, K. Itoh, F. Miko, Y. Sawaki, H. Iwamura, A. Izuoka, and T. Sugawara, *J. Am. Chem. Soc.* **112,** 4074 (1990).
8. T. Ishida and H. Iwamura, *J. Am. Chem. Soc.* **113,** 4238 (1991).
9. N. Nakamura, K. Inoue, and H. Iwamura, *Angew. Chem. Int. Ed. Engl.* **32,** 873 (1993).
10. N. Ventosa, D. Ruiz, C. Rovira, and J. Veciana, *Mol. Cryst. Liq. Cryst.* **232,** 333 (1993).
11. A Rajca, S. Utamapanya, and S. Thayumanavan, *J. Am. Chem. Soc.* **114,** 1884 (1992).
12. G. Blondin and J. J. Girerd, *Chem. Rev.* **90,** 1359 (1989), and reference there in.
13. G. Christou, *Acc. Chem. Res.* **22,** 328 (1989).
14. S. J. Lippard, *Angew. Chem. Int. Ed. Engl.* **30,** 34 (1991).
15. K. L. Taft, G. C. Papaefthymiou, and S. J. Lippard, *Inorg. Chem.* **33,** 1510 (1994).
16. M. T. Pope, "Heteroply and Isopoly Oxometalates." Spinger-Verlag, Berlin, 1983.
17. J. M. Clemente-Juan and E. Coronado, *Coord. Chem. Rev.* **193–195,** 361 (1999).
18. J. J. Borrás-Almenar, J. M. Clemente, E. Coronado, and B. S. Tsukerblat, *Chem. Phys.* **195,** 1 (1995).
19. J. J. Borrás-Almenar, J. M. Clemente, E. Coronado, and B. S. Tsukerblat, *Chem. Phys.* **195,** 16 (1995).
20. J. J. Borrás-Almenar, J. M. Clemente, E. Coronado, and B. S. Tsukerblat, *Chem. Phys.* **195,** 29 (1995).
21. E. Coronado and V. Laukhin, J. R. Galán-Mascarós C. J. Gómez-García, *Nature* **408,** 447 (2000).
22. C. Zener, *Phys. Rev.* **82,** 403 (1951).
23. P. W. Anderson and H. Hasegawa, *Phys. Rev.* **100,** 675 (1955).
24. B. S. Tsukerblat, M. I. Belinskii, and V. E. Fainziberg, Magnetochemistry and spectroscopy of transition metal exchange clusters, in "Soviet Sci. Rev. Section B: Chemistry Reviews" (M. E. Vol' pin, Ed.), Vol. 9, p. 337. Harwood Academic, New York, 1987.
25. J. J. Borrás-Almenar, J. M. Clemente, E. Coronado, A. V. Palii, T. S. Tsukerblat, and R. Georges, *in* "Localized and Itinerant Molecular Magnetism: From Molecular Assemblies to the Devices," (E. Coronado, P. Delhaès, D. Gatteschi, and J. S. Miller, Eds.), NATO. ASI Series, Vol. E-321, p. 105. Kluwer Academic, Dordrecht, 1996.
26. B. S. Tsukerblat, "Group Theory in Chemistry and Spectroscopy." Academic Press, London, 1994.
27. D. Gatteschi, O. Kahn, J. S. Miller, and F. Palacio (Eds.) "Magnetic Molecular Materials," NATO ASI Series E: Applied Science, Vol. 198. Kluwer Academic, Dordrecht, 1991.
28. E. Coronado, P. Delhaès, D. Gatteschi, and J. S. Miller (Eds.) "Localized and Itinerant Molecular Magnetism: From Molecular Assemblies to the Devices," NATO ASI Series, Vol. E-321. Kluwer Academic, Dordrecht, 1996.
29. W. E. Hatfield, *in* "Theory and Applications of Molecular Paramagnetism" (E. A. Boudreaux and L. N. Mulay, Eds.) Wiley, New York, 1976.
30. A. Bencini and D. Gatteschi, "Electron Paramagnetic Resonance of Exchange Coupled Systems." Springer-Verlag, New York, 1990.
31. O. Kahn, "Molecular Magnetism." VCH, New York, 1993.

32. J. J. Borrás-Almenar, J. M. Clemente-Juan, E. Coronado, and B. S. Tsukerblat, *Inorg. Chem.* **38,** 6081 (1999).
33. M. Drillon, L. Padel, and J. C. Berrier, *J. Chem. Soc. Faraday Trans. 2* **75,** 1193 (1979).
34 G. J. Wessel and J. J. W. Ijdo, *Acta Crystallogr.* **10,** 466 (1957).
35. B. Briat, O. Kahn, I. Morgenstern-Badarau, and J. C. Rivoal, *Inorg. Chem.* **20,** 4193 (1981).
36. M. Drillon and R. Georges, *Phys. Rev. B* **26,** 3882 (1982).
37. D. I. Khomskii and K. I. Kugel, *Sov. Phys. Usp.* **136,** 231 (1982).
38. M. Drillon and R. Georges, *Phys. Rev. B* **24,** 1278 (1981).
39. B. Leuenberger and H. U. Güdel, *Mol. Phys.* **51,** 1 (1984).
40. J. J. Borrás-Almenar, J. M. Clemente-Juan, E. Coronado, A. V. Palii, and B. S. Tsukerblat, *J. Phys. Chem. A* **102,** 200 (1998).
41. J. J. Borrás-Almenar, J. M. Clemente-Juan, E. Coronado, A. V. Palii, and B. S. Tsukerblat, *J. Chem. Phys.* **114,** 1 (2001).
42. J. J. Borrás-Almenar, J. M. Clemente-Juan, E. Coronado, A. V. Palii, and B. S. Tsukerblat, *J. Chem. Phys.* **254,** 275 (2000).
43. A. Ceulemans, L. F. Chibotaru, G. A. Heylen, K. Pierloot, and L. G. Vanquickenborne, *Chem. Rev.* **100,** 787 (2000).
44. A. Ceulemans, G. A. Heylen, L. F. Chibotaru, L. T. Maes, K. Pierloot, C. Ribbing, and L. G. Vanquickenborne, *Inorg. Chim. Act.* **251,** 15 (1996).
45. K. Y. Wong and P. N. Schatz, *Prog. Inorg. Chem.* **28,** 369 (1981).
46. S. B. Piepho, *J. Am. Chem. Soc.* **110,** 6319 (1990).
47. J. J. Borrás-Almenar, E. Coronado, S. M. Ostrovsky, A. V. Palii, and B. S. Tsukerblat, *J. Chem. Phys.* **240,** 149 (1999).
48. S. B. Piepho, *J. Am. Chem. Soc.* **112,** 4197 (1990).
49. J. J. Borrás-Almenar, J. M. Clemente-Juan, E. Coronado, V. Yu Mirovitskii, A. V. Palii, and B. S. Tsukerblat in "Vibronic Interactions: Jahn-Teller effect in Colossal Magnetoresistance and Related Phenomena," (M. Kaplan and G. Zimmerman, Eds.) Kluwer, Dordrecht, 2001.
50. J. J. Borrás-Almenar, J. M. Clemente-Juan, E. Coronado, A. V. Palii, and B. S. Tsukerblat, *J. Chem. Phys.* **114,** 1 (2001).
51. S. Sugano, Y. Tanabe, and H. Kamimura, "Multiplets of Transition Ions in Cystals." Academic Press. New York, 1970.
52. R. Saillant and R. A. D. Wentworth, *Inorg. Chem.* **7,** 1606 (1968).
53. A. Ceulemans, L. F. Chibotaru, G. A. Heylen, and K. Pierloot, *Mol. Phys.* **97,** 1197 (1999).